

High-intensity ultrasound catheter ablation achieves deep mid-myocardial lesions in vivo

Babak Nazer, MD,* David Giraud, MEng,* Yan Zhao, MD,* James Hodovan, MS,*
Miriam R. Elman, MPH, MS,*[†] Ahmad Masri, MD, MS,*
Edward P. Gerstenfeld, MD, MS, FHRS,[‡] Jonathan R. Lindner, MD*

From the *Knight Cardiovascular Institute, Oregon Health and Science University, Portland, Oregon,
[†]School of Public Health, OHSU/Portland State University, Portland, Oregon, and [‡]Division of
Cardiology, University of California San Francisco, San Francisco, California.

BACKGROUND Radiofrequency ablation of epicardial and mid-myocardial ventricular arrhythmias is limited by lesion depth.

OBJECTIVE The purpose of this study was to generate deep mid-interventricular septal (IVS) lesions using high-intensity ultrasound (US) from an endocardial catheter-based approach.

METHODS Irrigated US catheters (12 F) were fabricated with 3×5 mm transducers of 5.0, 6.5, and 8.0 MHz frequencies and compared in an *ex vivo* perfused myocardial ablation model. *In vivo* septal ablation in swine ($n = 12$) was performed via femoral venous access to the right ventricle. Lesions were characterized by echocardiography, cardiac magnetic resonance imaging, and electroanatomic voltage mapping pre- and post-ablation, and at 30 days. Four animals were euthanized immediately post-ablation to compare acute and chronic lesion histology and gross pathology.

RESULTS In *ex vivo* models, maximal lesion depth and volume was achieved by 6.5 MHz catheters, which were used *in vivo*. Lesion depth by gross pathology was similar post-ablation (10.8 mm; 95% confidence interval [CI] 9.9–12.4 mm) and at 30 days (11.2

mm; 95% CI 10.6–12.4 mm) ($P = .56$). Lesion volume decreased postablation to 30 days (from 255 [95% CI 198–440] to 162 [95% CI 133–234] mm³; $P = .05$), yet transmuralities increased from 58% (95% CI 50%–76%) to 81% (95% CI 74%–93%), attributable to a reduction in IVS thickness (from 16.0 ± 1.7 to 10.6 ± 2.4 mm; $P = .007$). Magnetic resonance imaging confirmed dense septal ablation by delayed enhancement, with increased T1 time post-ablation and at 30 days and increased T2 time only post-ablation. Voltage mapping of both sides of IVS demonstrated reduced unipolar (but not bipolar) voltage along the IVS.

CONCLUSION High-intensity US catheter ablation may be an effective treatment of mid-myocardial or epicardial ventricular arrhythmias from an endocardial approach.

KEYWORDS Catheter ablation; Mid-myocardial; Ultrasound; Ventricular arrhythmia; Ventricular tachycardia

(Heart Rhythm 2021;■:1–9) © 2020 Heart Rhythm Society. All rights reserved.

Introduction

Ventricular arrhythmias (VAs) often arise from deep mid-myocardial or epicardial sites, particularly in patients with nonischemic cardiomyopathy^{1,2} or those with idiopathic VAs from the left ventricular (LV) summit.³ Radiofrequency (RF) ablation is limited by shallow depth (1.9–6.7 mm),^{4–6} often precluding mid-myocardial ablation or epicardial ablation from an endocardial approach. Furthermore, RF ablation

of the basal interventricular septum (IVS) from a right ventricular (RV) approach may increase the risk of damage to the His-Purkinje system, which is often subendocardial in location.⁷

Therapeutic high-intensity ultrasound (HIU) is achieved by applying ultrasound (US) energy, often in the diagnostic frequency range (1–10 MHz) but at sufficiently high amplitude (~ 10 MPa) to generate localized tissue heating and thermal necrosis.⁸ By virtue of the natural focusing and deep tissue penetration of US energy, HIU ablation has been shown to demonstrate deep, nearly transmural lesions from an epicardial approach, while sparing the immediately adjacent tissue.⁹ The application of HIU for arrhythmias has focused primarily on epicardial US device placement, which allows ablation without near-field injury to epicardial vessels.^{9,10} HIU ablation from an endocardial approach has not been fully explored, but has the potential to make deep mid-myocardial lesions from an endocardial catheter location. The sparing of the near-field myocardium during HIU ablation may also be advantageous for avoiding damage

Dr. Nazer is supported by a grant (K08-HL138156) from the National Institutes of Health (NIH; United States). Dr. Nazer and Mr Giraud are supported by an E21 Physician-Engineer Partnership Award from the American Society of Echocardiography (Durham, NC). Dr. Lindner is supported by grants (R01-HL078610, R01-HL130046, and P51-OD011092) from the NIH. The rest of the authors report no conflicts of interest. This study was partially supported by an investigator-initiated grant from Biosense-Webster International (United States). **Address reprint requests and correspondence:** Dr. Babak Nazer, Knight Cardiovascular Institute, Oregon Health and Science University, 3181 SW Sam Jackson Park Rd, Portland, OR 97239. E-mail address: nazer@ohsu.edu.

to the His-Purkinje system when performing ablation of the IVS from an RV approach.

In this study, we designed, fabricated, acoustically characterized, optimized, and tested HIU ablation catheters suitable for ablation of the IVS from a femoral venous approach to the RV. We hypothesized that this approach could produce deep mid-myocardial lesions without His-Purkinje injury and iatrogenic atrioventricular (AV) block.

Methods

Catheter assembly and acoustic testing

Side-facing HIU ablation catheters were fabricated from piezoelectric crystals, electrical cable, modified stainless steel tubing, nylon tubing, and electrical connectors (Figure 1A). Each catheter contained a planar 5.0, 6.5, and 8.0 MHz single-element PZT-4 piezoceramic crystal 3×5 mm in dimension (EBL Products Inc., East Hartford, CT), which was soldered to 34 AWG micro coaxial electrical cable (Alpha-wire, Elizabeth, NJ) and a BNC connector (Amphenol, Wallingford, CT). Edges of the US crystal were bonded to a partially cut stainless steel hypodermic tubing that served as a rigid transducer platform with air backing. The transducer platform assembly was then bonded to 12-F flexible nylon catheter tubing (Freelin-Wade Inc., McMinnville, OR). The transducer assemblies were encapsulated within a thin-walled polyester balloon through which closed-loop internal irrigation was performed with deionized and degassed water at 10°C with a flow rate of 50 mL/min supplied by a peristaltic pump. Finally, impedance matching networks were built to achieve >99% electrical power transmission.

Catheters were operated in the continuous wave mode using signals produced by a waveform generator (Agilent 33250A, Santa Clara, CA), amplified by a power amplifier (Amplifier Research 600A225, Souderton, PA), and monitored using a high-voltage passive detection US probe (LeCroy PPE 1.2 kV, Chestnut Ridge, NY) connected to an oscilloscope (LeCroy Waverunner 44 MXi-A, Chestnut Ridge, NY). After fabrication, the US pressure field for each catheter was characterized in filtered, deionized, and degassed water at room temperature using a needle hydrophone (75 μ m, Precision Acoustics, Dorchester, UK) to map peak negative acoustic pressures (Figure 1B-C).

Ex vivo myocardial ablation protocol

Ovine hearts were obtained from animals receiving intravenous heparin immediately before killing. Hearts were studied within 30 minutes of explantation. A 5-F perfusion catheter was sutured in the proximal left anterior descending coronary artery (LAD) to perfuse the anterior myocardium. The heart was suspended in a degassed water bath at room temperature. A solution of 1% bovine serum albumin in normal saline was perfused through the LAD at 30 mL/min using a non-peristaltic syringe pump. Epicardial HIU lesions were applied at a power of 30 W for 60 seconds. Eight separate lesions were made in the LAD perfusion territory: one anteroseptal line of 4 extending from the basal to the apical anteroseptum 1 cm lateral and

parallel to the LAD and a second anterior line of 4 just 1 cm lateral to the first line. US frequency ($n = 32$ sonications for each frequency) was randomized on a per-heart basis.

In vivo myocardial ablation protocol

This study was approved and monitored by the Oregon Health & Science University Institutional Animal Care and Use Committee under guidelines set forth by the Association for Assessment and Accreditation of Laboratory Animal Care International and consistent with the *Guide for the Care and Use of Laboratory Animals (National Research Council)*. Female farm swine (*Sus domesticus*) (40–45 kg) were anesthetized with tiletamine and zolazepam and intubated. Anesthesia was maintained with inhaled isoflurane (1.5%–3.5% via 2 L/min O₂). Isothermia was maintained with water-heated blankets. The HIU catheter was advanced via femoral venous access through a 14-F steerable sheath to the RV and guided to the RV septum using fluoroscopic and transthoracic echocardiography (TTE) guidance. Eight sonications at a power of 30 W were performed for 60 seconds, approximately 1 cm apart in a 4×2 pattern with 4 lesions extending from the basal to mid-anteroseptum and a second row from the basal to mid-inferoseptum. Continuous electrocardiographic monitoring was performed during the procedure, with attention to AV conduction, QRS width, and morphology. Four swine were euthanized immediately post-ablation per protocol for the assessment of acute lesions. The remainder were survived for 30 days.

Imaging and electroanatomic mapping

TTE (Epiq CV, Philips Ultrasound, Andover, MA) was performed with a phased array probe and tissue harmonic filtering pre-ablation, immediately post-ablation, and, when applicable, at 30 days. Parasternal short-axis views at the basal and mid-ventricular planes and apical 4-chamber views were obtained at a transmit frequency of 1.6 MHz.

A subset of swine underwent cardiac magnetic resonance imaging (MRI) preablation ($n = 4$), immediately post-ablation ($n = 6$), and at 30 days ($n = 6$). MRI was performed on a 3.0 T Siemens Prisma system (Erlangen, Germany) using the body coil for RF transmitting as well as spine and body matrix coils for signal receiving and with electrocardiographic gating. After standard T1- (spin-lattice relaxation time) and T2- (spin-spin relaxation time) weighted scans, 0.1 mmol/kg of ProHance gadolinium contrast agent (Bracco, Milan, Italy) was administered intravenously. First-pass perfusion as well as T1-weighted delayed enhanced images were acquired ~20 minutes postinjection with phase-sensitive inversion recovery reconstruction. MRI analysis was performed using dedicated MRI software (Circle Cardiovascular Imaging, Calgary, Canada). The number of lesions and their locations were first assessed on short-axis slices of delayed enhancement images. The corresponding regions on the native (precontrast) T1 and T2 maps were sampled for T1 and T2 times at lesion locations. We used MODified Look Locker Inversion recovery (MOLLI sequences) to measure T1. These measurements were also

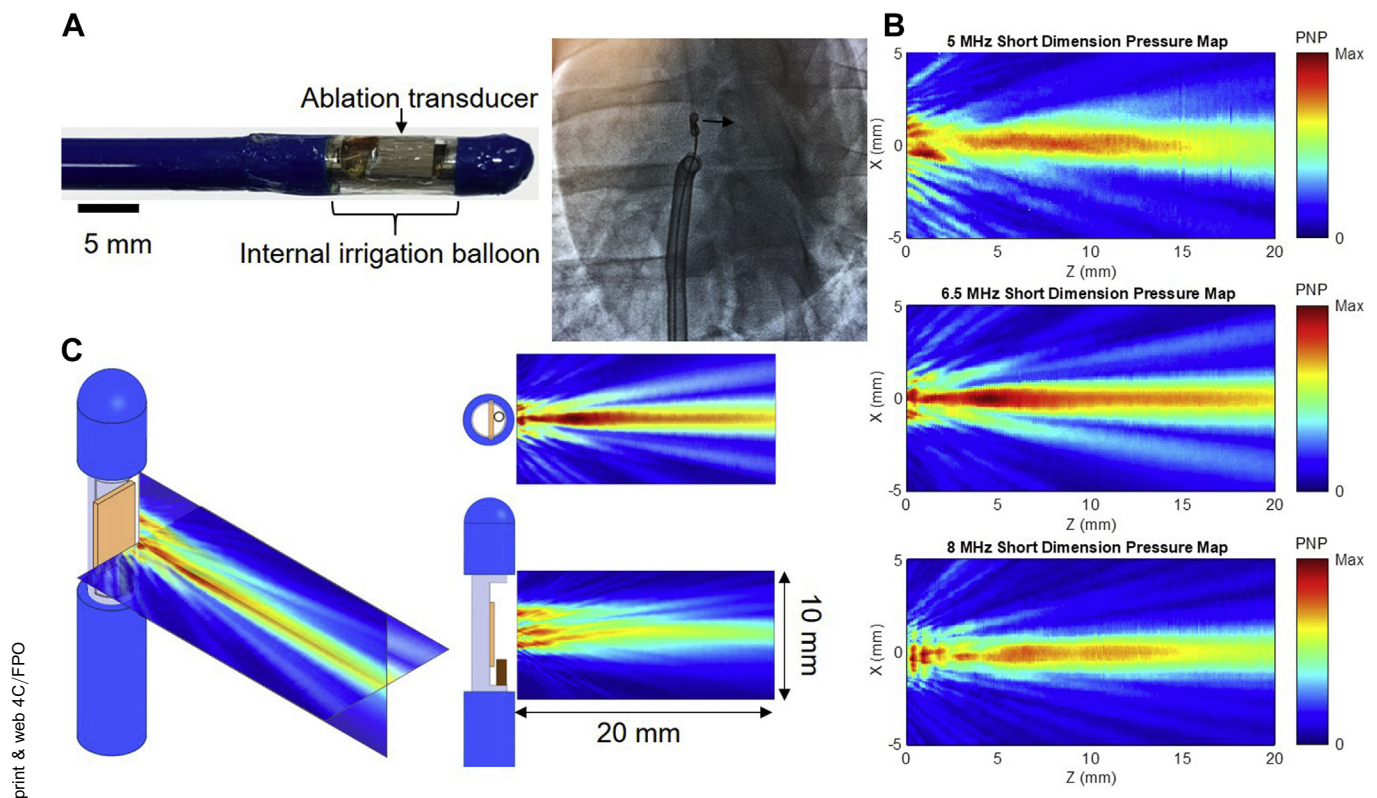


Figure 1 High-intensity ultrasound (HIU) catheter and acoustic fields. **A:** Twelve-French internally irrigated HIU catheters were built and directed to the right ventricular septum under transthoracic echocardiogram and fluoroscopic guidance (left anterior oblique 15° view demonstrates the transducer in the profile and aiming toward the septum). **B:** Acoustic field maps measured using a needle hydrophone in degassed water, where the catheter surface is at $Z = 0$ mm and HIU pressure propagates in the positive Z direction, indicating the 6.5 MHz (middle) catheter to generate the deepest lesions and largest acoustic field. **C:** Further characterization of the 6.5 MHz HIU catheter's acoustic field in 2 orthogonal planes. PNP = peak negative pressure.

normalized to their respective T1 and T2 times directly opposite in the non-ablated, inferolateral LV myocardium to account for variations between swine. T1 and T2 times were made in the middle third of the ventricular myocardium to avoid partial volume effects.

Electroanatomic voltage mapping of the RV and LV septum was also performed in a subset of 4 swine using the PentaRay catheter (Biosense Webster International, Diamond Bar, CA) pre- and post-ablation and at 30 days. Bipolar voltage mapping was assessed at the standard threshold of 0.5 and 1.5 mV and unipolar voltage mapping at 1.0 and 5.5 mV for the RV septum and 1.0 and 8.3 mV for the LV septum.

Gross pathology and histology

For both *ex vivo* and *in vivo* studies, the heart was perfused with 10 g of 2,3,5-triphenyl-2H-tetrazolium chloride in 50 mL of saline (through the perfusion catheter for *ex vivo* studies and via central venous access for *in vivo* studies) to aid visual inspection of myocardial necrosis. Hearts were fixed in 10% formalin at 4°C for 1 week and then sectioned in 3-mm-thick short-axis segments. Segments containing lesions were further sectioned to measure individual lesion sizes in 3 dimensions and then further fixed and stained with Masson's trichrome and hematoxylin and eosin.

Lesion depth was measured starting from and orthogonal to the RV endocardium and ending at the distal (toward the LV)

end of the lesion (Figure 2B). RV subendocardial sparing measurement also started at the RV endocardium, but extended toward the proximal (toward the RV) end of the lesion (Figure 2B). Lesion volume was calculated using the visual observation of lesion boundaries as input to the revolved ellipsoid volume formula ($4/3 \times \pi \times L/2 \times W/2 \times T/2$), where L is the lesion length (measured in the axis going away from the transducer from the RV to the LV endocardium), W is the width (from the antero- to the inferoseptum), and T is the thickness (along the basal-to-apical axis). This equation has been validated for the assessment of ablation lesions.¹⁰ *SLesion transmural* (defined as percentage of the IVS thickness bounded by the lesion at its cross-section) and near-field (RV side of the mid-septum) vs far-field (LV side of the mid-septum) deposition of necrosis was quantified by determining the IVS midline with a custom image processing algorithm using spline analysis (Online Supplement).

For histological analysis of necrosis, inflammatory infiltrate, hemorrhage, and fibrosis, lesion blocks were further sectioned at a thickness of 10 μ m and stained with hematoxylin and eosin and Masson's trichrome.

Statistical analysis

Data were analyzed using GraphPad Prism software (version 8.4.1; San Diego, CA) and SAS (version 9.4; Cary, NC). Groupwise differences were assessed using the

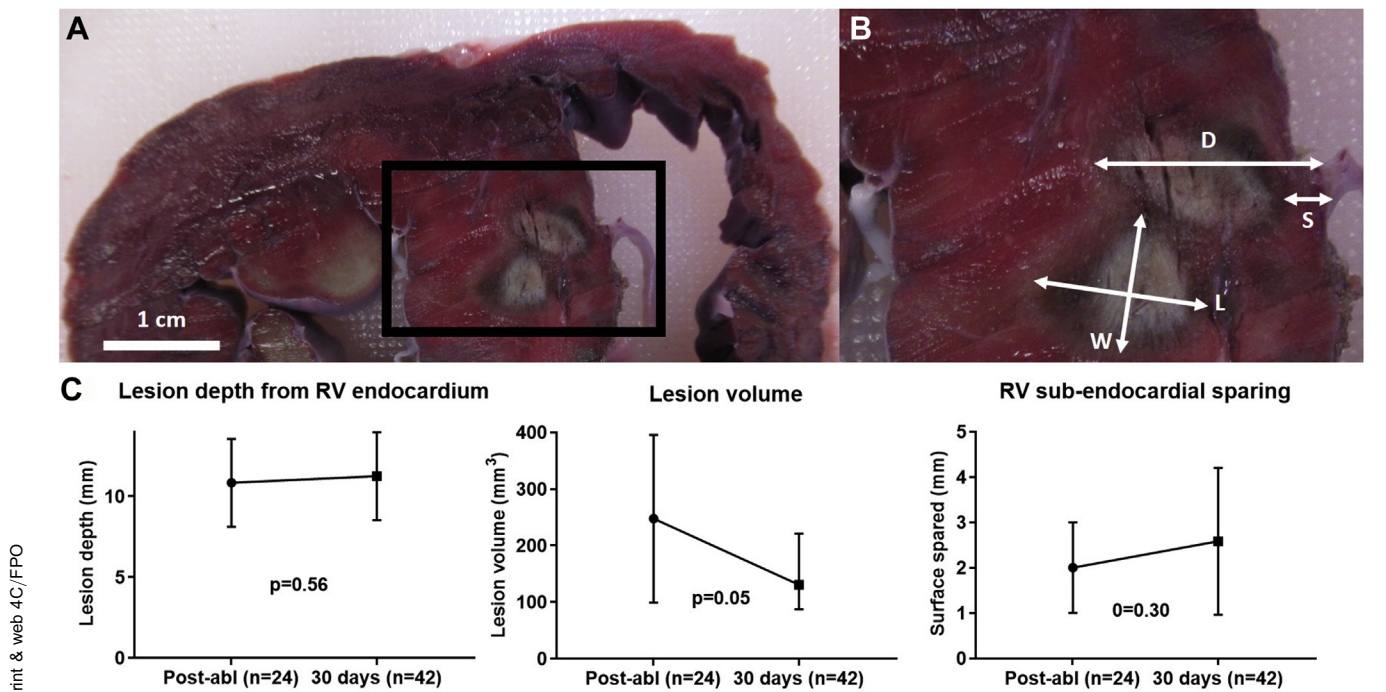


Figure 2 In vivo myocardial lesion characteristics. **A:** Short-axis gross pathology of 2 adjacent lesions in the interventricular septum (IVS). **B:** Magnification of IVS demonstrating lesion measurements (D, depth; S, subendocardial surface sparing; L, length; W, width; T, thickness is not shown, but was measured by sectioning serial short-axis cross-sections). **C:** Quantification of gross pathological lesion characteristics. Graph bars represent means, and error bars represent SD. RV = right ventricular.

Mann-Whitney *U* test for data that were determined to be nonnormally distributed. For data with normal distribution, groupwise differences were assessed using the Student *t* test (paired for comparisons at different time points) or analysis of variance (ANOVA). These data are presented as mean \pm SD. A 1-way analysis of variance test was used when comparing multiple groups per time points. One survival swine died at 14 days. Gross pathological data from this swine were included with the 30-day survival swine. When comparing repeated measures (multiple ablation lesions per animal) among multiple swine, fixed effects regression models were fit and SEs adjusted to address the correlation among measurements from the same animal. Means with bootstrapped 95% confidence intervals (CIs) based on 500 replications are reported from these models. All statistical tests were 2-sided, with $P \leq .05$ considered significant.

Results

Comparison of US frequencies

The acoustic fields of HIU catheters with fundamental frequencies of 5.0, 6.5, and 8.0 MHz were mapped (Figure 1) and predicted that 6.5 MHz would generate the largest and deepest acoustic field. Ablation at 5 MHz did not reproducibly result in necrotic lesions (32 sonications yielded only 4 identifiable small lesions on gross pathology), likely because of the reduced thermal effects of US at lower frequencies having fewer harmonics formed during nonlinear acoustic propagation.^{11,12} Ablation at 6.5 MHz generated lesions that were deeper (10.7 ± 3.2 mm vs 8.3 ± 2.6 mm from the RV endocardium; $P = .0015$) and larger in volume (223 ± 171 mm³ vs

137 ± 95 mm³ in volume; $P = .028$) than at 8 MHz (Online Supplemental Figure 1). Sparing of the RV subendocardial surface tissue immediately adjacent to the transducer was similar between both frequencies (1.6 ± 1.2 mm vs 1.5 ± 0.6 mm distance from the RV endocardial surface to ablation lesion; $P = .797$). To increase the study efficiency, in vivo studies were performed only with 6.5 MHz HIU catheters.

In vivo ablation: Pathological analysis

In the 4 animals euthanized after immediate post-ablation imaging, histology detected 24 necrotic lesions out of 32 HIU ablation attempts (75% efficiency); while 42 necrotic lesions were found out of 64 HIU ablation attempts (66% efficiency) in survival animals. Sonication locations that were more apically located were least likely to result in visible lesions on gross pathology, largely because of the inability of the custom steerable sheath to reach the apical septum.

HIU lesions were typically ellipsoid in shape (Figure 2), similar to prior descriptions of HIU epicardial LV lesions, and in contrast to the typical half-ellipsoid shape of RF lesions.⁹ The mean lesion depth was similar immediately post-ablation (10.8 mm; 95% CI 9.9–12.4 mm) and at 30 days (11.2 mm; 95% CI 10.6–12.4 mm) ($P = .56$), although lesion volume decreased over time (from 255 [95% CI 198–440] to 162 [95% CI 133–234] mm³; $P = .05$) (Figure 2). The RV subendocardial surface was similarly spared at both time points (2.2 mm; 95% CI 1.7–3.3 mm vs 2.7 mm; 95% CI 2.3–3.4 mm; $P = .3$). Similar to lesion depth, lesion length (L, going away from the transducer from the RV to the LV endocardium and excluding RV subendocardial sparing) was similar at both

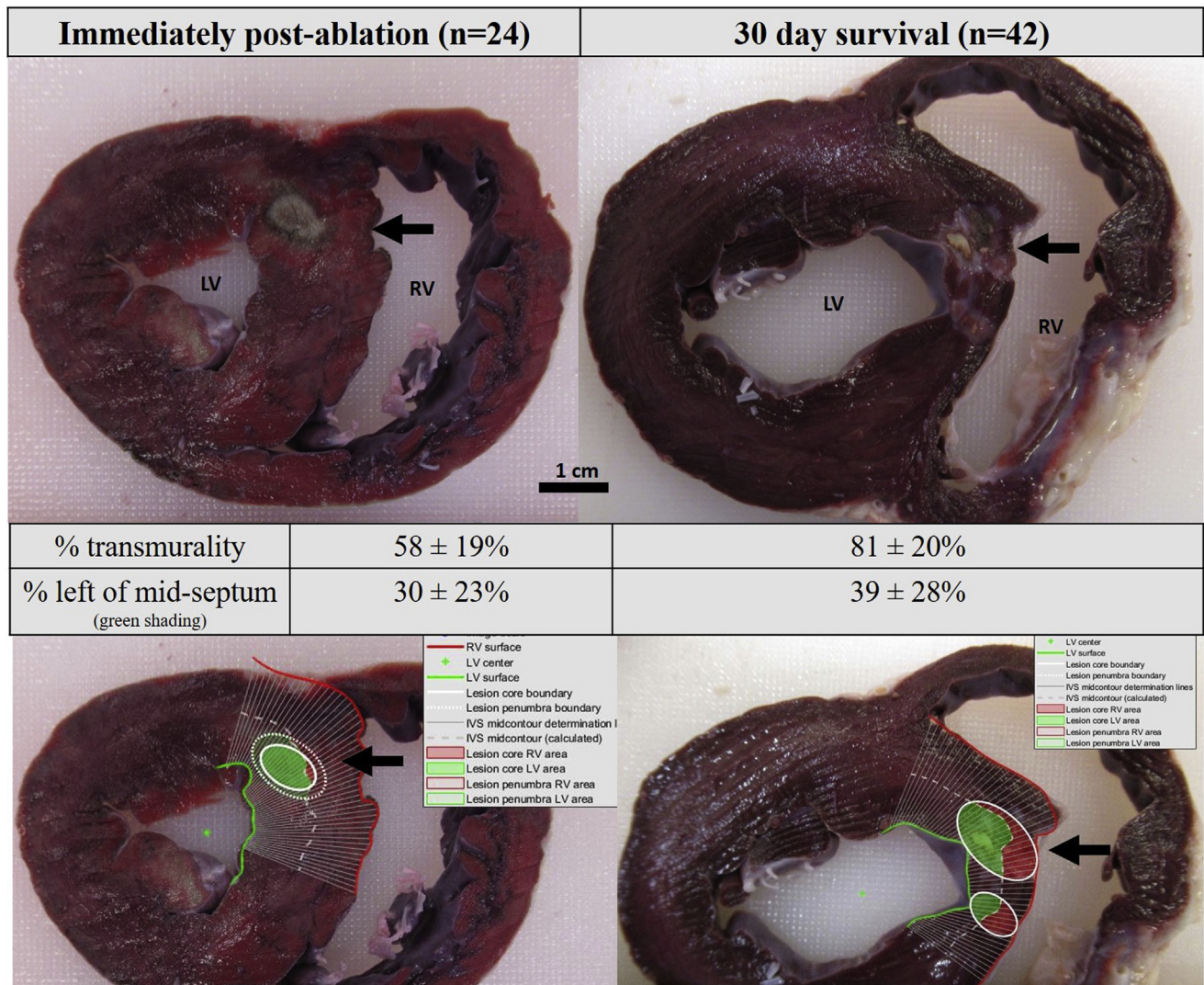


Figure 3 Gross pathology images of *in vivo* lesions immediately postablation (**left**) and at 30 days (**right**). Bottom row images demonstrate image processing with spline analysis defining the portion of the lesion surface area to the right (RV; red) and left (LV; green) ventricular side of the septum, with the mid-septum defined as the white dotted line.

time points. However, lesion width (W) decreased from 6.4 (95% CI 5.9–7.0) to 5.5 (95% CI 5.0–6.1) mm ($P = .006$) and lesion thickness (T) decreased from 7.8 (95% CI 7.2–8.4) to 6.2 (95% CI 5.6–6.8) mm at 30 days ($P < .0001$).

Based on spline analysis image processing, a similar portion of the lesion surface area was deposited on the LV side of the IVS (30%; 95% CI 22%–46% postablation vs 39%; 95% CI 33%–51% at 30 days; $P = .29$) (Figure 3). Spline analysis showed that lesion transmuralty increased from 58% (95% CI 50%–76%) to 81% (95% CI 74%–93%) over 30 days ($P = .002$). Increased transmuralty despite decreased lesion volume at 30 days compared with immediately post-ablation was attributable to IVS remodeling resulting in reduced thickness: IVS thickness at the level of the lesions decreased from 16.0 ± 1.7 mm post-ablation to 10.6 ± 2.4 mm at 30 days ($P = .0074$) (Figure 3).

Histology demonstrated myocyte disruption without fibrosis or inflammation immediately post-ablation. At 30

days, dense midseptal fibrosis was noted without a surrounding inflammatory infiltrate (Online Supplemental Figure 2).

TTE, MRI, and electroanatomic mapping

TTE confirmed gross pathological findings: diastolic IVS thickness by TTE increased from 11.8 ± 1.3 mm at baseline to 13.4 ± 1.6 mm ($P = 0.002$) immediately post-ablation (presumably because of edema) but decreased to 10.0 ± 1.3 mm at 30 days ($P = .0003$ by ANOVA for between-group differences; $P = 0.004$ for comparison between pre-ablation and 30 days post-ablation) despite swine growth. The LV ejection fraction at baseline was $58\% \pm 6\%$, decreased to $49\% \pm 4\%$ immediately postablation (due to hypokinesis of the basal IVS), and recovered to $58\% \pm 5\%$ at 30 days ($P = .0002$ by ANOVA for between-group differences; $P = .92$ for comparison between pre-ablation and 30 days post-ablation).

MRI also confirmed IVS remodeling: IVS thickness increased from 11.0 ± 0.8 mm at baseline to 13.8 ± 1.7

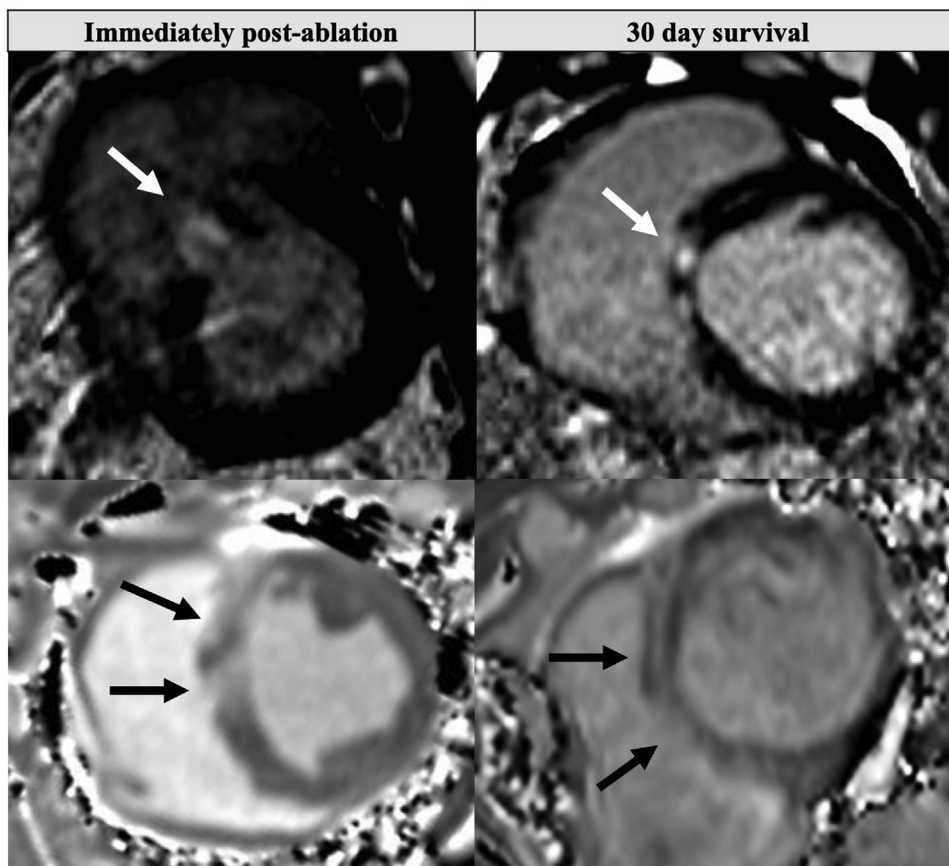


Figure 4 Short-axis magnetic resonance imaging images of high-intensity ultrasound (HIU) lesions immediately postablation (**left**) and at 30 days (**right**). Late gadolinium enhancement in the septum (*top row*) corresponded to increased precontrast T1 time (*bottom row*). Ablation had been performed from the right ventricle in the direction of *white arrows*.

mm immediately postablation (presumably because of edema) but decreased to 10.6 ± 1.1 mm at 30 days ($P = .003$ by ANOVA) despite swine growth. First-pass MRI contrast perfusion imaging demonstrated dense perfusion defects in the basal to mid-IVS immediately post-ablation (Online Supplemental Videos 1 and 2). Late gadolinium enhancement (LGE) detected areas of HIU ablation in the IVS, but resolution was insufficient to quantify individual lesion size on a per-lesion basis: 3.6 ± 1.1 regions of LGE were present post-ablation and 3.4 ± 1.1 regions at 30 days (Figure 4; Online Supplemental Figure 3), likely because of the coalescence of multiple HIU lesions into single LGE regions. T1 time at the basal IVS HIU ablation sites increased from 1176 ± 18 ms preablation to 1408 ± 87 ms postablation and remained elevated at 30 days (1319 ± 128 ms; $P = .008$ by ANOVA). T2 time increased from 40.4 ± 5.1 to 64.2 ± 6.0 ms postablation but then returned to near baseline 47.1 ± 5.8 ms at 30 days ($P = .1169$ for comparison between pre-ablation and 30 days; $P < .0001$ by ANOVA for groupwise comparison). Data were similar when normalizing septal ablation site T1 and T2 values with basal inferolateral (non-ablated) T1 and T2 values.

Electroanatomic voltage mapping did not reveal any bipolar voltage abnormalities at standard voltage thresholds, but demonstrated new areas of reduced unipolar voltage along the basal and mid-RV septum immediately post-ablation

(10.6 ± 6.1 cm²) and at 30 days (7.0 ± 3.5 cm²) ($P = .35$). Similar unipolar voltage findings were present in the LV septum (7.6 ± 0.5 cm² vs 6.0 ± 1.8 cm²; $P = .31$) confirming deep lesions (Figure 5). No fractionated or late electrograms were noted, suggesting fairly homogeneous, deep ablation.

Procedural complications

No AV block, QRS widening, pericardial effusions, or ventricular septal defects were noted intra- or post-procedure. All survival swine recovered uneventfully from anesthesia after the procedure. One survival swine died suddenly at 14 days postprocedure, with no structural abnormalities determined at autopsy.

Discussion

There are spatial challenges related to catheter ablation of VAs. Mid-myocardial sites of VA origin and epicardial sites of origin in patients unsuitable for percutaneous subxiphoid pericardial access pose significant challenges for RF ablation. Several novel strategies have arisen to improve upon shallow lesion depth of standard RF ablation, including an RF needle catheter,¹³ stereotactic body radiation therapy,¹⁴ use of hypotonic irrigated RF ablation,¹⁵ bipolar RF ablation,^{16,17} and

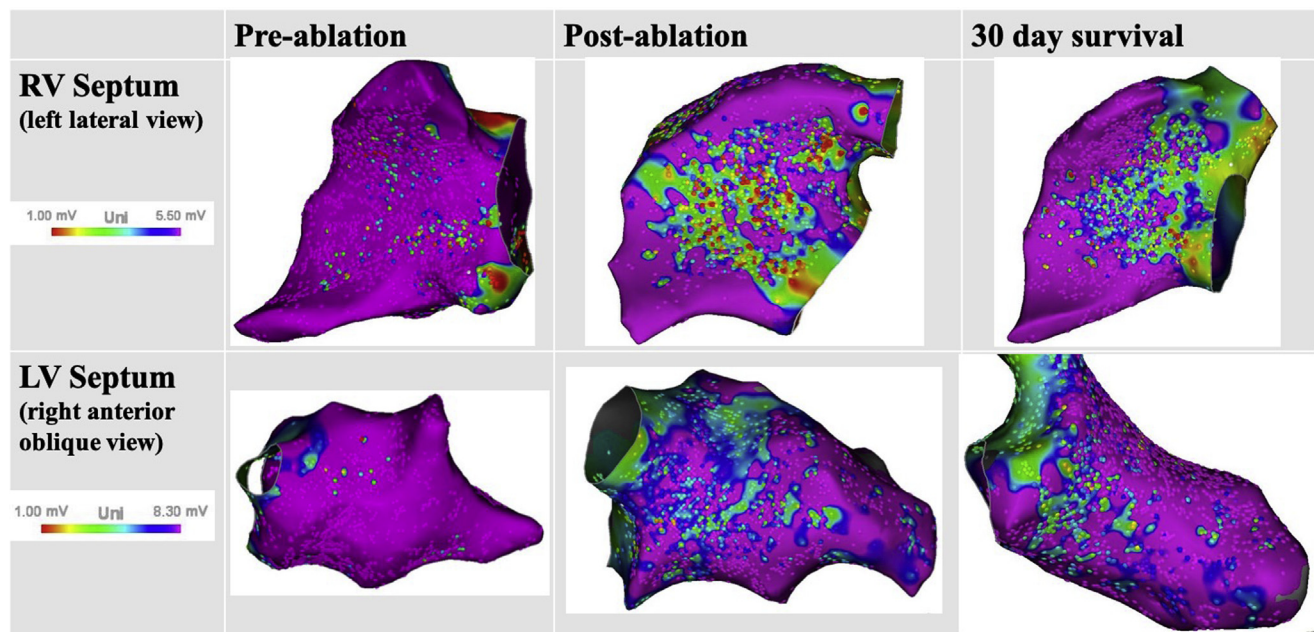


Figure 5 Electroanatomic unipolar voltage mapping of the right (RV) and left (LV) ventricular septum. New unipolar voltage abnormalities noted postablation and at 30 days, confirming the presence of deep mid-myocardial lesions.

alcohol venous ablation,¹⁸ although access to these therapies is limited, and recurrence and complication rates remain high.

There are several potential advantages of using HIU over RF for targeting mid-myocardial and epicardial sites from the endocardium. Lower US absorption in tissue allows deeper penetration. Moreover, US transducers can be geometrically focused, or the natural focus of the flat US element may permit an “offset” that, with catheter cooling by irrigation, can spare tissue immediately adjacent to the transducer, thereby avoiding the subendocardial His-Purkinje system with septal ablation. Finally, US-based ablation may permit the real-time monitoring of the region of thermal injury that could help guide lesion placement or size.

In our study, HIU ablation from the RV side of the IVS resulted in lesions of ~11 mm depth, initially spanning 58% of the IVS acutely increasing to 81% transmural at 30 days. This increase in transmural was, in part, explained by remodeling of the IVS, which was noted to markedly decrease in thickness in response to septal ablation. Indeed, 38% of the lesion surface area was deposited on the far-field, LV side of the IVS, with the first 2–3 mm of the RV septal subendocardium spared. No QRS widening, bundle branch block, or AV block was noted, suggesting protection of the subendocardial His-Purkinje system. However, it should be noted that while extensive ablation of the basal-mid RV anterosseptum was performed, sonications were not performed in a dedicated manner over the His and right bundle potentials, but simply in their general region. Furthermore, we did not histopathologically define the His-Purkinje system after euthanasia and thus were unable to define the proximity of our ablation lesions to the conduction system. No acute complications were noted, but there was 1 autopsy-negative sudden death event at 14 days that we presume was due to VA secondary to

heterogeneous necrosis in the IVS with lesions spaced 1 cm apart, although late AV block cannot be excluded.¹⁹

HIU lesions were successfully identified by cardiac MRI, which may serve as a means of assessing lesion extent clinically using either LGE or noncontrast T1 imaging, as has previously been shown for RF.²⁰ In our study, T1 and T2 times at the IVS were both elevated immediately post-ablation whereas only T1 time remained elevated at 30 days, suggesting an acute edematous and/or inflammatory reaction (although significant inflammation not noted histologically post-ablation), resolving to dense, mid-septal fibrosis without edema or inflammation at 30 days (which was confirmed by histology). It should be noted that our MRI lacked the resolution to confidently measure individual lesion dimensions for correlation with gross pathology.

Limitations of our study include lack of an RF control group, although the shallow depth of RF ablation has been well-documented,^{4–6} including in our prior study⁹ where it was 4.7 ± 4.0 mm and significantly less deep than epicardial HIU. Swine were not monitored with telemetry or implantable loop recorder monitoring over the 30-day survival period; we cannot exclude delayed transient AV block. We also did not test a large range of frequencies, transducer sizes (restricted to 3×5 mm transducers that would accommodate a 12-F catheter), or differences in acoustic power or lesion duration time. Instead, we used HIU frequencies within a range known to promote thermal necrosis²¹ and our previous experience to narrow our range of HIU variables, compared 5, 6.5, and 8 MHz in ex vivo models, which identified 6.5 MHz as the optimal frequency for the transducer size in the in vivo study.

Another limitation is the large variability in lesion sizes. While TTE was used to confirm placement against the RV

endocardial surface, we cannot exclude the periodic noncontact, which could explain the variability as well as why lesion efficiency was not 100% (ie, fewer histological lesions than ablation procedures performed; most evident for sonications made in the most apical portions of the RV) and also why lesion size varied. Furthermore, our side-facing transducer may not have always been exactly parallel to the IVS. Future iterations of the catheter should use a contact- and orientation-sensing mechanism. Integration of the catheter into electroanatomic mapping may also aid in assessing contact as well as allow us to guide HIU ablation directly over the His-Purkinje system to formally demonstrate sparing of the conduction system with surface-sparing lesions. Finally, our studies were not performed in a model of arrhythmia or cardiomyopathy. It has been shown that RF applications within the myocardial scar are less likely to generate reliable and large necrotic lesions compared with applications performed in healthy myocardium because of heterogeneous electrical impedance of scar tissue.²² HIU thermal necrosis relies on tissue *acoustic* impedance, which is more homogeneous across tissue types than electrical impedance.²³ Thus, HIU lesions may perform more efficiently in scar, although this has yet to be tested.

Future investigations of HIU should assess lesions in large animal cardiomyopathy models, use long-term ambulatory rhythm monitoring for proarrhythmia, and assess endocardial to epicardial lesions with ablation over the non-septal LV endocardium. While we previously demonstrated a dose-response relationship between HIU powers of 15–30 W and lesion depth and volume⁹ (and thus chose 30 W for this study as it is the maximal acoustic power that the transducer and circuitry can tolerate in the continuous wave mode), further control of lesion depth and size may also be achieved with adjusting transducer size or ablation time and should be investigated. Our finding of reduction in IVS thickness is intriguing and warrants further investigation with a consolidated lesion set over the basal septum to determine whether HIU may be a suitable approach for septal reduction therapy in hypertrophic cardiomyopathy.

Conclusion

This first study of HIU endocardial ventricular ablation demonstrates deep, nearly transmural mid-myocardial lesion formation with sparing of the subendocardium and His-Purkinje system.

Acknowledgments

We thank Xin Li, PhD, William Woodward, MS, Chris Diederich, PhD, and Peter Douglas Jones, BS, for their technical assistance. We also thank Traci L. Schaller BS, LVT, LAT, for veterinary and anesthesia care and Thomas Murphy, BA for assistance with electroanatomic mapping.

Appendix Supplementary data

Supplementary data associated with this article can be found in the online version at <https://doi.org/10.1016/j.hrthm.2020.12.027>.

References

- Oloriz T, Silberbauer J, MacCubelli G, et al. Catheter ablation of ventricular arrhythmia in nonischemic cardiomyopathy: anteroseptal versus inferolateral scar sub-types. *Circ Arrhythm Electrophysiol* 2014;7:414–423.
- Haqqani HM, Tschabrunn CM, Tzou WS, et al. Isolated septal substrate for ventricular tachycardia in nonischemic dilated cardiomyopathy: incidence, characterization, and implications. *Heart Rhythm* 2011;8:1169–1176.
- Romero J, Shivkumar K, Valderrabano M, et al. Modern mapping and ablation techniques to treat ventricular arrhythmias from the left ventricular summit and interventricular septum. *Heart Rhythm* 2020;17:1609–1620.
- Jauregui-Abularach ME, Campos B, Betensky BP, Michele J, Gerstenfeld EP. Comparison of epicardial cryoablation and irrigated radiofrequency ablation in a swine infarct model. *J Cardiovasc Electrophysiol* 2012;23:1016–1023.
- John RM, Connell J, Termin P, et al. Characterization of warm saline-enhanced radiofrequency ablation lesions in the infarcted porcine ventricular myocardium. *J Cardiovasc Electrophysiol* 2014;25:309–316.
- D'Avila A, Houghtaling C, Gutierrez P, et al. Catheter ablation of ventricular epicardial tissue: a comparison of standard and cooled-tip radiofrequency energy. *Circulation* 2004;109:2363–2369.
- Nagarajan VD, Ho SY, Ernst S. Anatomical considerations for His bundle pacing. *Circ Arrhythm Electrophysiol* 2019;12:e006897.
- Nazer B, Gerstenfeld EP, Hata A, Crum LA, Matula TJ. Cardiovascular applications of the therapeutic ultrasound. *J Interv Card Electrophysiol* 2014;39:287–294.
- Nazer B, Salgaonkar V, Diederich CJ, et al. Epicardial catheter ablation using high-intensity ultrasound: validation in a swine model. *Circ Arrhythm Electrophysiol* 2015;8:1491–1497.
- Koruth JS, Dukkupati S, Carrillo RG, et al. Safety and efficacy of high-intensity focused ultrasound atop coronary arteries during epicardial catheter ablation. *J Cardiovasc Electrophysiol* 2011;22:1274–1280.
- Swindell W. A theoretical study of nonlinear effects with focused ultrasound in tissues: an “acoustic bragg peak.” *Ultrasound Med Biol* 1985;11:121–130.
- Hynynen K, Roemer R, Anhalt D, et al. A scanned, focused, multiple transducer ultrasonic system for localized hyperthermia treatments. *Int J Hyperthermia* 2010;26:1–11.
- Stevenson WG, Tedrow UB, Reddy V, et al. Infusion needle radiofrequency ablation for treatment of refractory ventricular arrhythmias. *J Am Coll Cardiol* 2019;73:1413–1425.
- Cuculich PS, Schill MR, Kashani R, et al. Noninvasive cardiac radiation for ablation of ventricular tachycardia. *N Engl J Med* 2017;377:2325–2336.
- Nguyen DT, Tzou WS, Sandhu A, et al. Prospective multicenter experience with cooled radiofrequency ablation using high impedance irrigant to target deep myocardial substrate refractory to standard ablation. *JACC Clin Electrophysiol* 2018;4:1176–1185.
- Koruth JS, Dukkupati S, Miller MA, Neuzil P, D'Avila A, Reddy VY. Bipolar irrigated radiofrequency ablation: a therapeutic option for refractory intramural atrial and ventricular tachycardia circuits. *Heart Rhythm* 2012;9:1932–1941.
- Nguyen DT, Tzou WS, Brunnequell M, et al. Clinical and biophysical evaluation of variable bipolar configurations during radiofrequency ablation for treatment of ventricular arrhythmias. *Heart Rhythm* 2016;13:2161–2171.
- Kreidieh B, Rodríguez-Mañero M, Schurmann P, Ibarra-Cortez SH, Dave AS, Valderrábano M. Retrograde coronary venous ethanol infusion for ablation of refractory ventricular tachycardia. *Circ Arrhythm Electrophysiol* 2016;9.
- Bleszynski PA, Goldenberg I, Fernandez G, et al. Risk of arrhythmic events after alcohol septal ablation for hypertrophic cardiomyopathy using continuous implantable cardiac monitoring. *Heart Rhythm* 2020;18:50–56.
- Kholmovski EG, Silvernagel J, Angel N, et al. Acute noncontrast T1-weighted magnetic resonance imaging predicts chronic radiofrequency ablation lesions. *J Cardiovasc Electrophysiol* 2018;29:1556–1562.
- Salgaonkar VA, Diederich CJ. Catheter-based ultrasound technology for image-guided thermal therapy: current technology and applications. *Int J Hyperthermia* 2015;31:203–215.

22. Barkagan M, Leshem E, Shapira-Daniels A, et al. Histopathological characterization of radiofrequency ablation in ventricular scar tissue. *JACC Clin Electrophysiol* 2019;5:920–931.
23. Sarvazyan AP, Rudenko OV, Swanson SD, Fowlkes JB, Emelianov SY. Shear wave elasticity imaging: a new ultrasonic technology of medical diagnostics. *Ultrasound Med Biol* 1998;24:1419–1435.